https://doi.org/10.5194/tc-2020-14
Preprint. Discussion started: 2 March 2020

The Cryosphere Discussions

Representative surface snow density on the East Antarctic Plateau

Alexander H. Weinhart[1], Johannes Freitag[1], Maria Hörhold[1], Sepp Kipfstuhl[1,2], Olaf Eisen[1,3]

[1] Alfred-Wegener-Institut Helmholtz-Zentrum für Polar- und Meeresforschung, Bremerhaven, Germany
[2] Physics of Ice, Climate and Earth, Niels Bohr Institute, University of Copenhagen, Copenhagen, Denmark
[3] Universität Bremen, Fachbereich Geowissenschaften, Bremen, Germany

Correspondence to: Alexander H. Weinhart (alexander.weinhart@awi.de)

Abstract

Surface mass balance estimates of polar ice sheets are essential to estimate the contribution of ice sheets to sea level rise, in response global warming. One of the largest uncertainties in the interior regions of the ice sheets, such as the East Antarctic Plateau (EAP), is the determination of a precise surface snow density. Wrong estimates of snow and firn density can lead to significant underestimations of the surface mass balance. We present density data from snow profiles taken along an overland traverse in austral summer 2016/17 covering over 2000 km on the Dronning Maud Land plateau. The sampling strategy included investigation on various spatial scales, from regional to local, with sampling locations 100 km apart as well as a high-resolution study in a trench at 30°E 79°S with thirty 3 m deep snow profiles. Density of the surface snow profiles has been measured volumetrically as well as using µ-computer tomography. With an error of less than 2%, the volumetric liner density provides higher precision than other sampling devices of smaller volume. With four spatially independent snow profiles per location we derive a representative and precise 1 m mean snow density with an error of less than 1.5%. The average liner density along the traverse across the EAP is 355 kg m^{-3}, which we identify as representative surface snow density between Kohnen station and Dome Fuji. The highest horizontal variability in density can be seen in the upper 0.3 m. Therefore, we do not recommend vertical sampling in intervals of less than several decimeters, as this does neither adequately cover seasonal variations in high accumulation areas nor the annual accumulation in low accumulation areas. From statistical analysis of the liner density on regional scale we identify representative spatial distributions of density based on geographical and thus climatic conditions. Our representative density of 355 kg m^{-3} is considerably different from the density of 320 kg m^{-3} provided by a regional climate model. This difference of more than 10% indicates the necessity for further calibration of density parameterizations. The difference in the total mass equivalent of measured and modelled density yields a 3% underestimation by models, which translates into 5 cm sea level equivalent. We do not find a statistically significant temporal trend in density changes over the last two decades. Our data provide a solid baseline for tuning parameterizations of the surface snow density for regions with low accumulation and low temperatures like the EAP to improve surface mass balance estimates of polar ice sheets.

https://doi.org/10.5194/tc-2020-14
Preprint. Discussion started: 2 March 2020


The Cryosphere Discussions

1 Introduction

Various future scenarios of a warming climate as well as current observations in ice sheet mass balance indicate a change in surface mass balance (SMB) on the Greenlandic and Antarctic ice sheets (IPCC, 2019). Accurate quantification of the current state and rate of change of SMB is therefore one of the most important quantities to estimate the contribution of the polar ice sheets to the global sea level rise (Lenaerts et al., 2019). Satellite altimetry is state of the art to measure height changes of the major ice sheets on large spatial scales (McMillan et al., 2014; Schroder et al., 2019; Sorensen et al., 2018). These changes are converted to a respective mass gain or loss, which are directly linked to an eustatic change in sea level (Rignot et al., 2019; Shepherd et al., 2018). But this estimate of a volume change converted to a mass change is impeded with large uncertainties (Shepherd et al., 2012). Apart from changes in bedrock elevation (Konrad et al., 2015; Sasgen et al., 2013), a precise estimation of the surface snow and firn density on top of the ice sheets, which undergoes constantly the natural process of densification, is crucial. Especially in the interior of the ice sheets the exact surface snow density is a limiting factor in precision. Due to the large extent of the ice sheets, the spatial coverage of in situ snow and firn density data is still sparse. To overcome this shortcoming, snow density is parameterized as a function of climatic conditions, such as temperature, wind speed and accumulation rate (Agosta et al., 2019; Kaspers et al., 2004) and validated with field measurements. But this parameterized approach (Ligtenberg et al., 2011; van den Broeke, 2008) seems to underestimate the real snow density when compared to independent in situ data from Antarctica (Sugiyama et al., 2012; Tian et al., 2018). Recently, Alexander et al. (2019) addressed the need for a precise snow density, especially in the uppermost meter, as its underestimation leads to significant surface mass balance errors. These data are urgently needed to optimize densification models (Lenaerts et al., 2019), which are crucial to calibrate altimetry data sets and therefore reduce the uncertainties in ice sheet mass balance estimates.

Arthern et al. (2006) derived snow accumulation in Antarctica from available in-situ measurements of accumulation and density. To obtain this density, sampling is usually conducted in snow pits with discrete sampling over depth. Between the stations Kohnen and Dome Fuji, snow density has been sampled in discrete depth intervals by Sugiyama et al. (2012), who report a high spatial variability on a kilometer scale. Small variability can be attributed to the sampling method. Conger and McClung (2009) compared different cutting devices with various volumes between 99 cm^3 and 490 cm^3. The combination of under-sampling (usually negligible), variation of the device itself (0.8-6.2%) and the weight error of the scale can add up to a significant error (dependent on the type up to 6%). Box- or tube-type cutters with larger sampling volumes are suggested for more precise measurements, with the disadvantage of coarser sampling intervals. Other methods to derive snow density with high precision but in discrete intervals have been used as well, measuring dielectric properties (Sihvola and Tiuri, 1986) or penetration force into the snow (Proksch et al., 2015).

Despite from climate-induced (e.g. seasonal or event-based) density fluctuations, surface snow density is also influenced by topographic changes of the ice sheet surface and underlying bedrock on small (tens of meters) and large spatial scales (up to hundreds of kilometers) (Frezzotti et al., 2002; Furukawa et al., 1996; Rotschky et al., 2004). Surface roughness and the surface

https://doi.org/10.5194/tc-2020-14
Preprint. Discussion started: 2 March 2020

slope in combination with dominant wind regimes and varying accumulation rates (Fujita et al., 2011) as well as stratigraphic noise (Fisher et al., 1985) cause additional variation in density.

In this paper, we present surface snow density data with high precision from a traverse covering over 2000 km on the East Antarctic Plateau (EAP). In order to avoid misunderstandings we follow Stenni et al. (2017) using the term EAP for the region higher than 2000 m above sea level (asl). The coldest 10 m firn temperature is recorded at Plateau Station (Picciotto et al., 1971), which makes the area the best modern analog of glacial firn. Within the framework of Coldest Firn (CoFi) project, we show snow density data using the recently introduced liner sampling method (Schaller et al., 2016), with a focus on the uppermost meter, as Alexander et al. (2019) pointed out the importance of precise 1 m snowpack density of polar ice sheets. To reduce the stratigraphic noise we show a different strategy with multiple samples per location. This allows a more precise determination of the local snowpack density. We discuss the representativeness of density on small and large scales. The spatial representativity of density profiles in East Antarctica has been recently addressed at the local scale (Laepple et al., 2016), but correlation studies for larger scales are currently not available. Beyond improving density retrieval, our results can be of particular interest for calibration of snow density parameterizations in this part of the East Antarctic ice sheet.

2 Material & methods

2.1 Study area

We performed an overland traverse in austral summer 2016/17 – a joint venture of the CoFi project and the Beyond EPICA – Oldest Ice Reconnaissance (OIR) pre-site survey (Karlsson et al., 2018; Van Liefferinge et al., 2018) (Fig 1). From Kohnen station the traverse went to former B51 drill site. Right after B51 the traverse split up and followed two different legs, to reunite at the OIR field camp at 79°S, 30°E. After accomplishing the OIR airborne survey the traverse continued to the former Plateau Station (abandoned in 1969) and then went back to Kohnen station.

https://doi.org/10.5194/tc-2020-14
Preprint. Discussion started: 2 March 2020

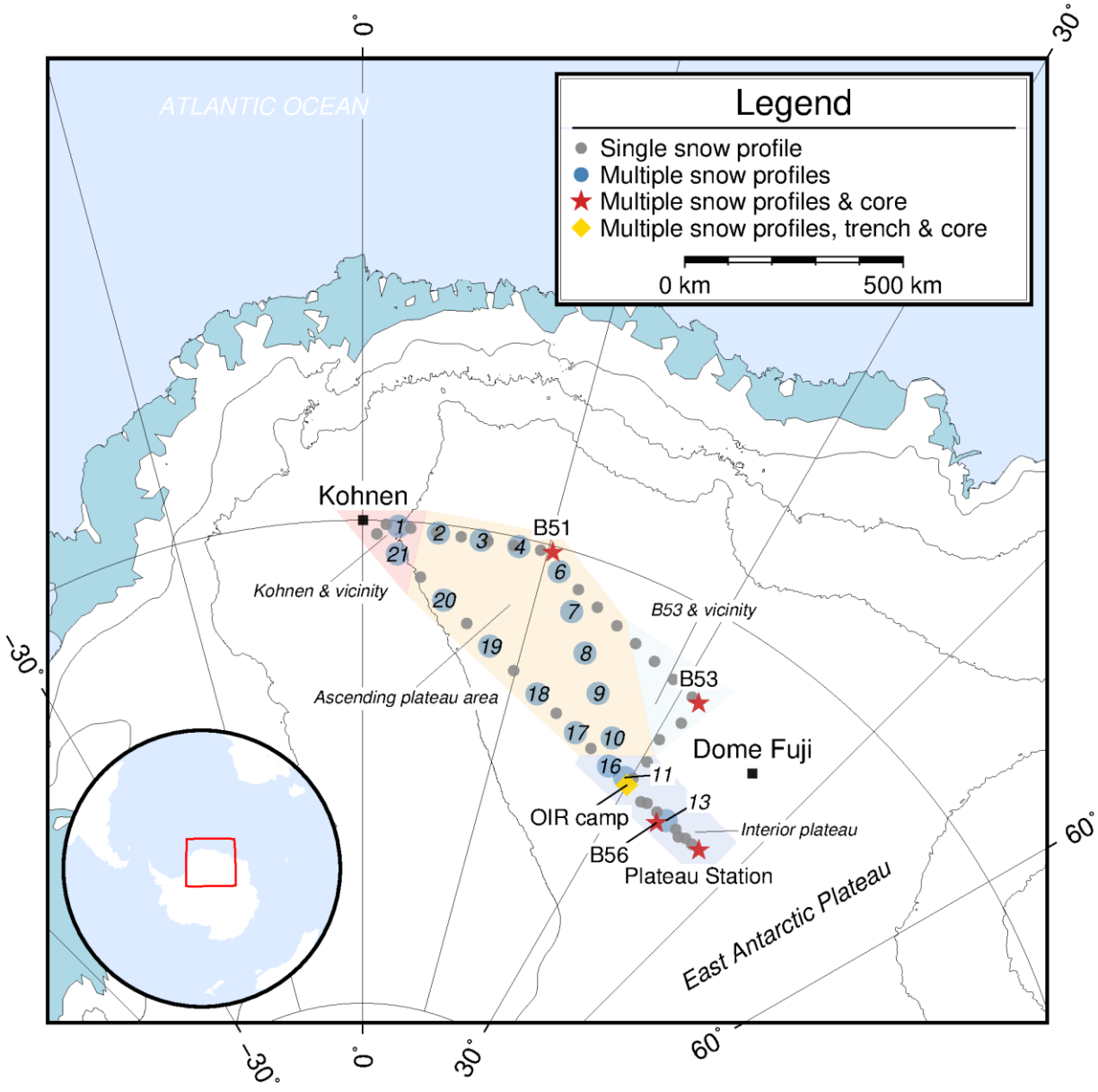

Figure 1: Overview map of the traverse route and sampling locations, inset shows location in Antarctica. The first sampling position with multiple liners after Kohnen station is named location 1. Following the traverse route, B51 is also called location 5, OIR camp location 12, Plateau Station location 14 and B56 location 15. 200 m firn cores were drilled at locations indicated with a red star. Subregions defined in chapter 2.5 are colored differently (Kohnen & vicinity: purple, ascending plateau area: orange, B53 & vicinity: light blue, interior plateau: lavender).

2.2 Liner sampling

For clarity, we define the terms used in the following paragraphs in Table 1.

https://doi.org/10.5194/tc-2020-14
Preprint. Discussion started: 2 March 2020

Table 1: Definition of terms used in the following sections are listed below

Term	*Symbol*	*Description*
Liner	-	1 m of snow sampled with a carbon fiber tube. This term is used in a methodological context or for the tube itself.
Snow profile	-	(Continuous) snow sample at a given position. It may consist of several consecutively (vertically on top of each other) sampled liners; the length can be 1-3 m.
Location	-	A given place with several snow profiles taken within a range of 50 m.
Liner mean density	ρ_L	Volumetrically derived 1 m average density of one single liner. Note: for snow profiles over 1 m length, liner mean densities for every meter segment are calculated individually.
µCT^x mean density	$\rho^x_{\mu CT}$	µCT derived mean density for the sampling interval x.
Location liner mean density	ρ_{loc}	Average of liner mean densities at one location for the same depth interval (usually 0-1 m).
Horizontal standard deviation	σ^x_H	Standard deviation of either liner means or µCT density for depth interval x over horizontal distance in a given area. Note: for 1 m we use the liner means, for smaller intervals µCT^x means.
Vertical standard deviation	σ^x_V	Vertical standard deviation of either µCT density over depth interval x or liner means (only for snow profiles >1 m) at a given position.
Standard error	σ_n	Definition in Sect. 2.4

Along the traverse route, vertical snow profiles were extracted using the snow liner sampling technique, described by Schaller et al. (2016). Each vertical profile was taken using a carbon fiber tube of one meter length and ten centimeters in diameter. The liner was pushed into the snow until the liner top was level with the snow surface. Afterwards, a snow pit next to the liner was dug and the snow was cut at the liner bottom with a metal plate to take the filled liner out of the pit wall. Both ends were covered with a WhirlPack® plastic bag to reduce possible contamination by touching the liner ends and air ventilation. During the sampling process, the liner was handled carefully to avoid concussions that destroy the original snow stratigraphy (e.g. not to bounce against the liner with the shovel and placing it softly into the sample box). A 1 m snow profile can be retrieved within 15 minutes.

In total 144 snow profiles in different setups and total lengths were taken (Sect. 2.2.1 – 2.2.3). The liners were stored in isolated polypropylene boxes and shipped to the Alfred Wegener Institute (AWI) in Bremerhaven in a continuous cold chain.

22 locations were sampled with multiple liners (usually four, at three locations the sample size was smaller), at 32 locations one single liner was taken (Fig. 1). Both strategies (single and multiple liners) have been sampled independently from each other.

2.2.1 Single snow profiles

Single liners were taken every 30 km. On the last segment of the traverse (OIR camp – Kohnen station) the distance increased due to limited liner availability. In total, 31 single snow profiles are available (Fig. 1).

https://doi.org/10.5194/tc-2020-14
Preprint. Discussion started: 2 March 2020

2.2.2 Multiple snow profiles

22 locations were sampled with multiple liners (usually four, at three locations the sample size was smaller) during overnight stops of the traverse, therefore the distance between the locations varied (roughly around 100 km). The four profiles were arranged in an even-sided triangular setup with one profile in the center (labeled with 'X') and three profiles around it (labeled with 'A', 'B' and 'C'). The corner profiles A, B, C are on a radius of 10 m to the central profile X (Fig. 2). 83 profiles were retrieved in this setup. The locations are named in ascending order (Fig. 1 and Tab. 2).

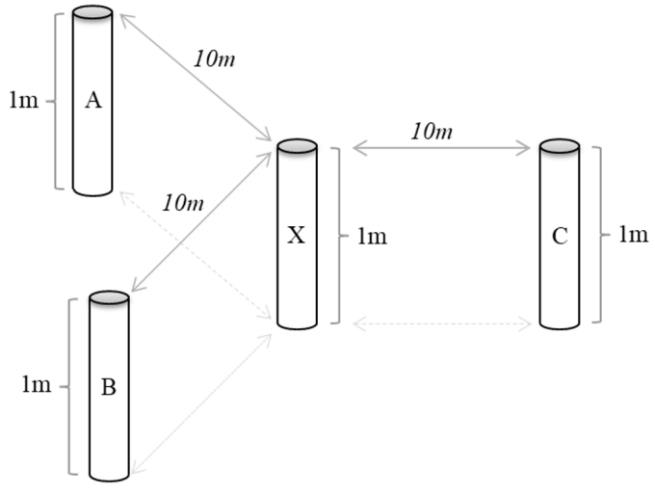

Figure 2: The sampling setup for locations with multiple snow profiles. The profiles A, B and C have a sampling distance of roughly 10 m to the central profile. Due to time or logistical constraints, locations 19 (three profiles) 11 and 13 (two profiles) have been sampled differently.

2.2.3 OIR trench

At the OIR camp (Fig. 1), a 50 meter long and ca. 2.3 meter deep trench was excavated with a PistenBully snow vehicle (Fig. 3). The trench orientation was perpendicular to the main wind direction (127° true North). Thirty 3 m snow profiles were sampled directly at the trench wall using the liner technique described above. At every sampling position in the trench three liners were taken below each other. The first liners were pushed into the snow around 0.2 meters behind the trench wall, to ensure an original stratigraphy not disturbed by excavation of the trench. After removal of the snow, the liners were directly taken out of the wall and the next consecutive liner in depth was placed at the same position (see Fig. 3, where the first liner is already in place). The lateral spacing between neighboring liners varied between 0.4 and 2.4 meters, depending on the surface structure. The total height difference between the lowest (first) and highest (last) profile is 0.385 m. The profiles were taken within two days after excavation of the trench. The trench surface was measured using optical levelling at the profile positions and in between two consecutive profiles.

https://doi.org/10.5194/tc-2020-14
Preprint. Discussion started: 2 March 2020

Figure 3: Sampling procedure in the OIR trench. The first carbon fiber liner is pushed into the snow after excavation of the trench. The positions were marked with a small bamboo pole. After retrieval of the first profile, the vertically consecutive second and third liners were taken. Two carbon fiber tubes lean at the trench wall. The last liner had to be dug out partly as the trench was only 2 to 2.5 meters deep.

2.3 Density measurements

The snow liners have been analyzed at AWI with the non-destructive micro-computer tomograph in a cold cell (µCT), specifically constructed for snow and ice cores. For technical details see Freitag et al. (2013) and Schaller et al. (2016).

Before the measurement all liners were weighted. The weight of the carbon fiber tube was subtracted. Then, ρ_L was calculated volumetrically. The exact height of filled snow inside the liner was determined using the µCT. All liners have been measured in a 2D-mode using a setup of 140 kV and 470 µA at -14°C. The µCT-density profiles have a vertical resolution of ca. 0.13 mm. Breaks and lost snow in the snow profiles haven been corrected.

Both, $\rho^{1m}_{\mu CT}$ and ρ_L are in good agreement with each other (Fig. 4), the differences between the volumetrically calculated ρ_L and $\rho^{1m}_{\mu CT}$ is on average only 0.6%. But for the calculation of the µCT density only the central segment of the liner is used as scattering effects at the outer parts of the liner occur. The used segment corresponds to less than half of the snow volume in the liner.

https://doi.org/10.5194/tc-2020-14
Preprint. Discussion started: 2 March 2020

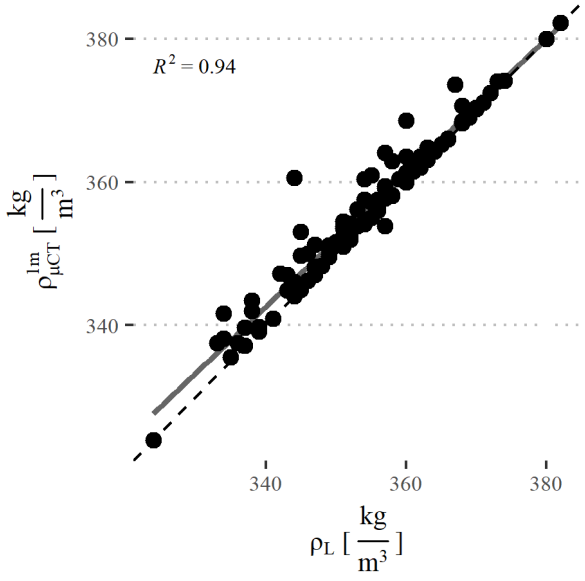

Figure 4: Comparison of ρ_L with $\rho^{1m}_{\mu CT}$ calculated from the 114 liners along the traverse. Values of both measurements are in good agreement with an R^2 of 0.94. The linear fit is given with a grey solid line, the dashed black line represents x=y.

Also ρ_L is affected by errors. Breaks that occurred during sampling or transport and lost snow in non-cohesive layers (such as depth hoar layers) or at the edges of the liner can lead to lower densities. Conger and McClung (2009) reported, that snow sampling devices with larger volumes usually result in higher precision in snow density. The volume of the snow liners (radius: 5 cm, length: 1 m) is 7855 cm³, 16 times the volume with the highest precision in their study.

As the volume error among single liners is not known, we assume a 0.3 mm variation in both dimensions (length and radius), resulting in a volume error around 1.2%. It is generally possible that at the liner top and bottom some snow is lost, but as the exact snow volume is determined with the µCT, we overcome this error source. As still small parts inside the liner might not be completely filled with snow (e.g. lost snow during the transport) we estimate the under-sampling error of the liner method to be less than 1.5%. Additional error sources are the precision of the used scale (1 g or 0.03% compared to the mean value along the traverse) as well as weight variations among the carbon tubes (<0.1%). An error estimation for an assumed maximum relative error for each part sums up to 1.9%.

Therefore, to quantify the 1 m snowpack density we use ρ_L, to investigate smaller intervals we use the $\rho^{1m}_{\mu CT}$ (Tab. 1).

2.4 Finding a representative density

Laepple et al. (2016) have shown, that snow profiles are spatially independent after 5-10 m sampling distance. To test how many liners per location are needed for a representative 1 m ρ_{loc}, we calculated σ^{1m}_H of ρ_{loc} using the maximum number of spatially independent ρ_L for ρ_{loc} (n). At the locations along the traverse we use all four available ρ_L to calculate ρ_{loc}. In the trench, we used two sets of seven ρ_L with a minimum sampling distance of adjacent profiles of 5 m and used the mean value

https://doi.org/10.5194/tc-2020-14
Preprint. Discussion started: 2 March 2020

of both sets. We can derive an error value, which depends on the number n of ρ_L at a given location. We divide σ^{1m}_H by $\sqrt{x}$, with x being a varying number of snow profiles from 2 to n-1. For instance, using seven profiles we are able to calculate the standard error for 2 to 6 profiles. This way we use the maximum sample size without an artificially caused bias in the data. We refer to the resulting term as standard error (σ_n) and aim for a density value with less than 2% relative σ_n.

2.5 Definition of subareas on the EAP

We pooled several snow profiles for further investigation to lower the influence of local noise and characterize the surface density of a larger (≥10,000 km²) region. We chose a minimum number of 10 profiles (0-1 m) per area. We followed the classification of Furukawa et al. (1996) as good as possible and used the 3500 m asl contour line as approximate boundary between different wind and accumulation regimes on the katabatic wind zone and the interior plateau (calm accumulation zone). This way we classified one major area "Ascending plateau area" (AP) with 64 profiles, covering roughly 140.000 km² between Kohnen station and OIR camp, and the smaller "Interior plateau" (IP) with 29 profiles between OIR camp and Plateau Station (28,500 km²). We did not include the OIR trench, as this specific location would have been overrepresented. The area around B53 (28,500 km²) was treated as a separate area as it is on the interior plateau close to the ice divide ("B53 & vicinity" – 10 profiles). Additionally, we handled the area around Kohnen station (Ko) with roughly 10,000 km² as another separate unit ("Kohnen & vicinity" – 45 profiles). The sample availability at Kohnen from other studies is sufficient, several liners from other sampling programs in seasons 2015/16 (16 profiles) and 2016/17 (18 profiles) have been added to the evaluation. Furthermore, a possible effect of the station itself should not be migrated into the other subsets. The areas are colored in the overview map (Fig. 1).

As we present density data on different scales, in this context we use the term 'local' scale for distances between profiles at one location and the area around a sampling location (i.e. tens of meters, Tab. 1). In contrast, the term 'regional' scale is used for distances between several locations (100 km to 1000 km) and areas in the dimensions of the subareas defined above. For all subsets, we present a spatial distribution of ρ_L and ρ_{loc}.

2.6 Optical levelling

At OIR camp and Plateau Station surface roughness along transects has been measured using optical levelling. The optical level was placed at the transect starting point. The first height measurement was done in 10 m distance to the starting point and repeated in 2 m intervals up to 58 m distance. In total six transects have been done at one location with 1 m lateral spacing between them.

https://doi.org/10.5194/tc-2020-14
Preprint. Discussion started: 2 March 2020

3 Results

3.1 Snow & firn density in the OIR trench

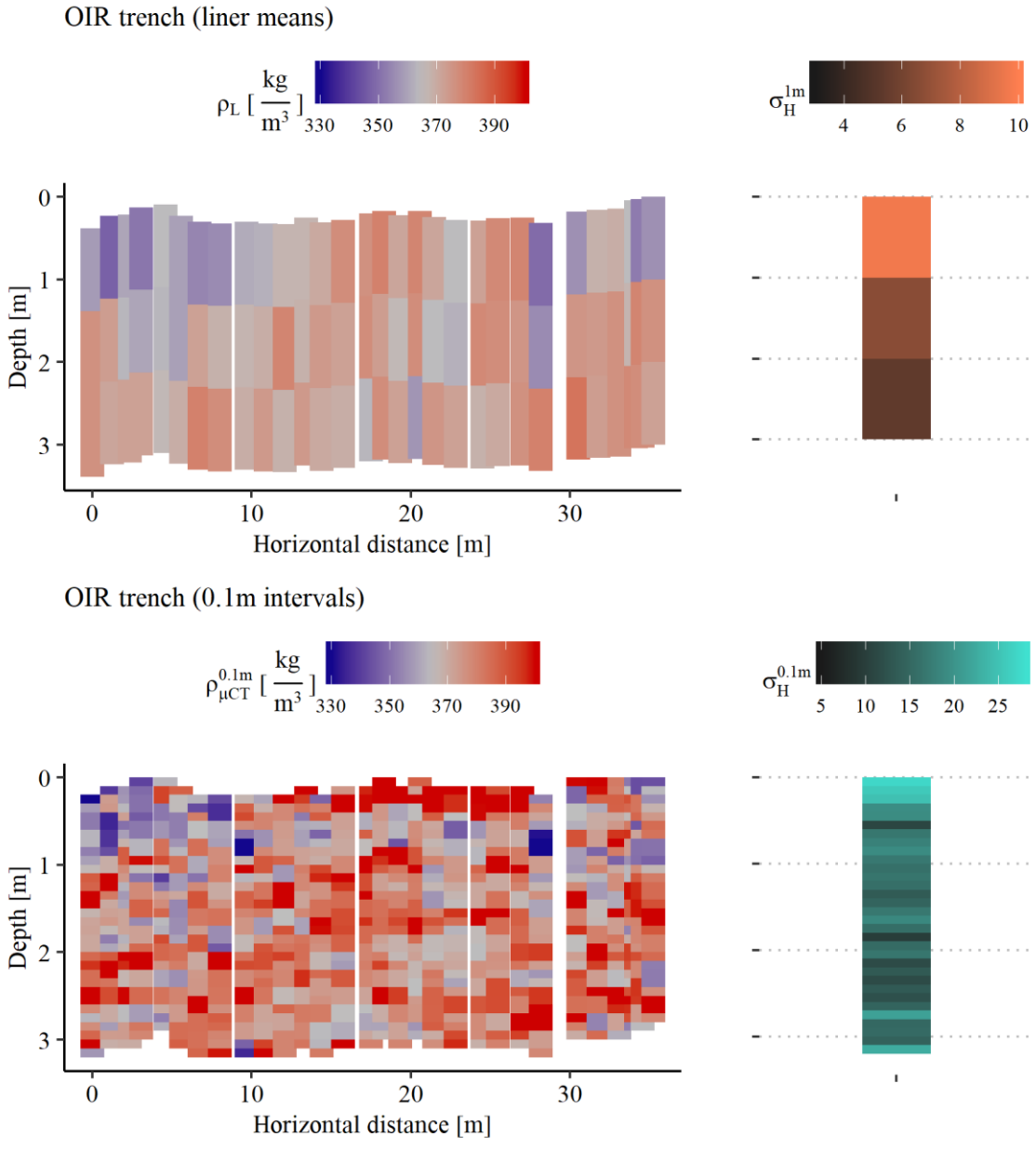

Figure 5: Density of the OIR trench from 30 profiles in vertical 1 m (liner means, top) and 0.1 m sampling intervals (µCT, bottom) in a color-coded plot. For the 0.1 m intervals, we applied a raster, starting at the highest profile (profile 30 at 35.22 m). ρ_L and $\rho^{0.1m}{}_{\mu CT}$, respectively, are given in a blue (low density) to red (high density) color code. On the right of each panel σ_H of the respective depth interval is shown. The highest horizontal variability can be seen in the uppermost part of the snow column (top meter and top 0.3 meters, respectively).

https://doi.org/10.5194/tc-2020-14
Preprint. Discussion started: 2 March 2020

ρ_L ranges in the OIR trench from 347 kg m^{-3} to 380 kg m^{-3}.We calculated ρ_{loc} for the OIR trench with 365±2 kg m^{-3}, which is 3.1% higher than for the whole traverse (Sect. 3.2). σ_H is in the range between 10 and 27 kg m^{-3} for 0.1 m sampling intervals and between 5 and 10 kg m^{-3} for 1 m sampling intervals (Fig. 5 and Tab. 4). The highest $\sigma^{0.1m}_H$ can be found in the top 0.3 m. σ^{3m}_V of the 3 meter profiles is 34 kg m^{-3} (Tab. 4).

3.2 Snow & firn density along the traverse

Here we present data from section 2.2.1 and 2.2.2. Along the traverse we find ρ_L ranging from 324 kg m^{-3} (pos. 22C) to 382 kg m^{-3} (pos. 16A). The average ρ_L (with standard error) calculated from 114 liners along the traverse is 354 ± 1 kg m^{-3} (Fig. 6).

ρ_{loc} (Tab. 1) is calculated from multiple snow profiles (Sect. 2.2.2) at each location. At location 21 and 1 we find the lowest ρ_{loc} with 344 and 345 kg m^{-3}, respectively. Highest ρ_{loc} is found at position 5 with 372 kg m^{-3} (Tab. 2). The average ρ_{loc} along the traverse is 355 ± 2 kg m^{-3}. To characterize the surface variability, we calculated σ^{1m}_H for each location separately. The average for the whole traverse is σ^{1m}_H=8 kg m^{-3}, ranging from minimum 2 kg m^{-3} at position 20 (and position 13 with only 2 profiles taken) to maximum 15 kg m^{-3} at position 22.

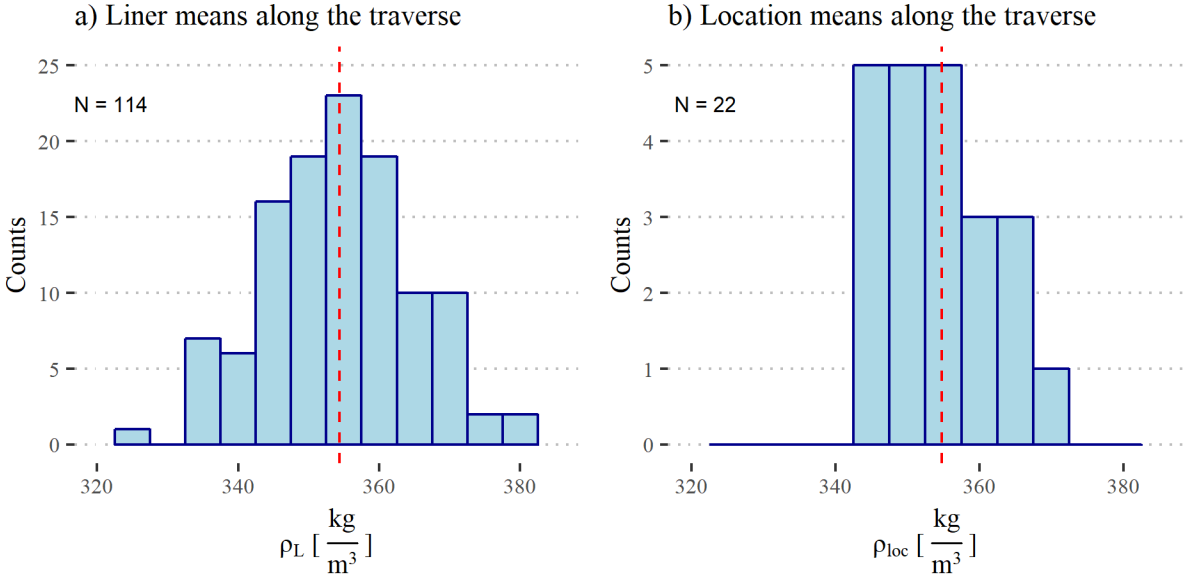

Figure 6: Histogram of a) ρ_L (0-1 m depth) and b) ρ_{loc} along the whole traverse route (profiles of the OIR trench not included). For both plots we used a bin width of 5 kg m^{-3}. The average liner mean and location mean, respectively, is given with the red dashed line.

A detailed overview of all ρ_{loc} and σ^{1m}_H along the traverse can be found in table 2.

https://doi.org/10.5194/tc-2020-14
Preprint. Discussion started: 2 March 2020

Table 2: ρ_{loc} at each location with multiple liners and the respective standard deviation. The number of liners at each location is given in brackets. For locations and abbreviations see Fig. 1.

Location (No. of ρ_L)	*Longitude [°]*	*Latitude [°]*	*Elevation [m asl]*	*ρ_{loc} [kg m^{-3}]*	*$\sigma^{1m}{}_H$ [kg m^{-3}]*
1 (4)	2.89	-75.11	2990	345	8
2 (4)	6.12	-75.18	3146	355	10
3 (4)	9.58	-75.21	3301	360	13
4 (4)	12.66	-75.18	3400	350	9
5 (4) – B51	15.4	-75.13	3470	372	7
6 (4)	16.32	-75.47	3484	353	14
7 (4)	18.33	-76.19	3463	346	8
8 (4)	20.66	-76.9	3456	355	9
9 (4)	23.19	-77.57	3452	351	12
10 (4)	26.3	-78.29	3455	346	5
11 (2)	29.38	-78.89	3461	350	6
12 (4) – OIR / B54	30.0	-79	3473	358	6
13 (2)	35.69	-79.18	3576	362	2
14 (4) – B55	40.56	-79.24	3665	352	10
15 (4) – B56	34.97	-79.33	3544	351	8
16 (4)	27.28	-78.84	3416	366	11
17 (4)	22.64	-78.5	3325	358	7
18 (4)	17.62	-78.02	3259	356	5
19 (3)	12.03	-77.32	3153	365	6
20 (4)	7.2	-76.54	3067	368	2
21 (4)	2.90	-75.67	2959	344	7
22 (4) – B53	31.91	-76.79	3737	345	15
Whole traverse (22 ρ_{loc})	-	-	-	355	8

3.3 Representativity of surface snow density on local scales

According to our calculation in the OIR trench, we get a value for σ_n of less than 1.5% of σ_n (4.9 kg m^{-3}) with four spatially independent snow profiles (Fig. 7). We note, that on average σ_n in the OIR trench is higher than the average of the four areal subsets (7.0 kg m^{-3} in contrast to 6.1 kg m^{-3} for two profiles and 5.7 kg m^{-3} in contrast 5.0 kg m^{-3} for three profiles). Unfortunately, we cannot test a number of profiles higher than six. But assuming a constant $\sigma^{1m}{}_H$, seven spatially independent profiles are needed to assure a relative σ_n of less than 1%.

https://doi.org/10.5194/tc-2020-14
Preprint. Discussion started: 2 March 2020

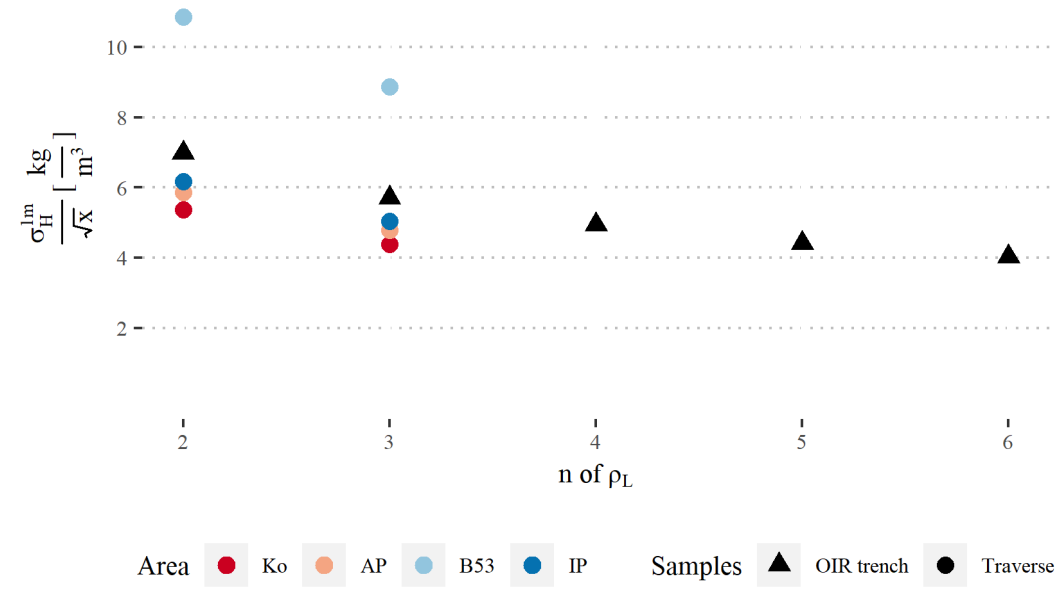

Figure 7: Standard error (σ_n) of σ_{loc} as a function of the number of liners (n). Triangles represent samples from the OIR trench while colored circles show samples along the traverse in the respective subsets (Sect. 2.5).

3.4 Representativity of surface snow density on regional scales

In the spatial density distribution of ρ_L and ρ_{loc}, find similar values for Kohnen & vicinity (352±1 kg m^{-3}), ascending plateau area (356±1 kg m^{-3}) and the interior plateau (355±2 kg m^{-3}) (Fig. 8). These have less than 1% difference from the average value of the whole traverse. Only B53 & vicinity shows lower density values (349±3 kg m^{-3}, -1.41% compared to the traverse mean density 354 kg m^{-3}).

https://doi.org/10.5194/tc-2020-14
Preprint. Discussion started: 2 March 2020

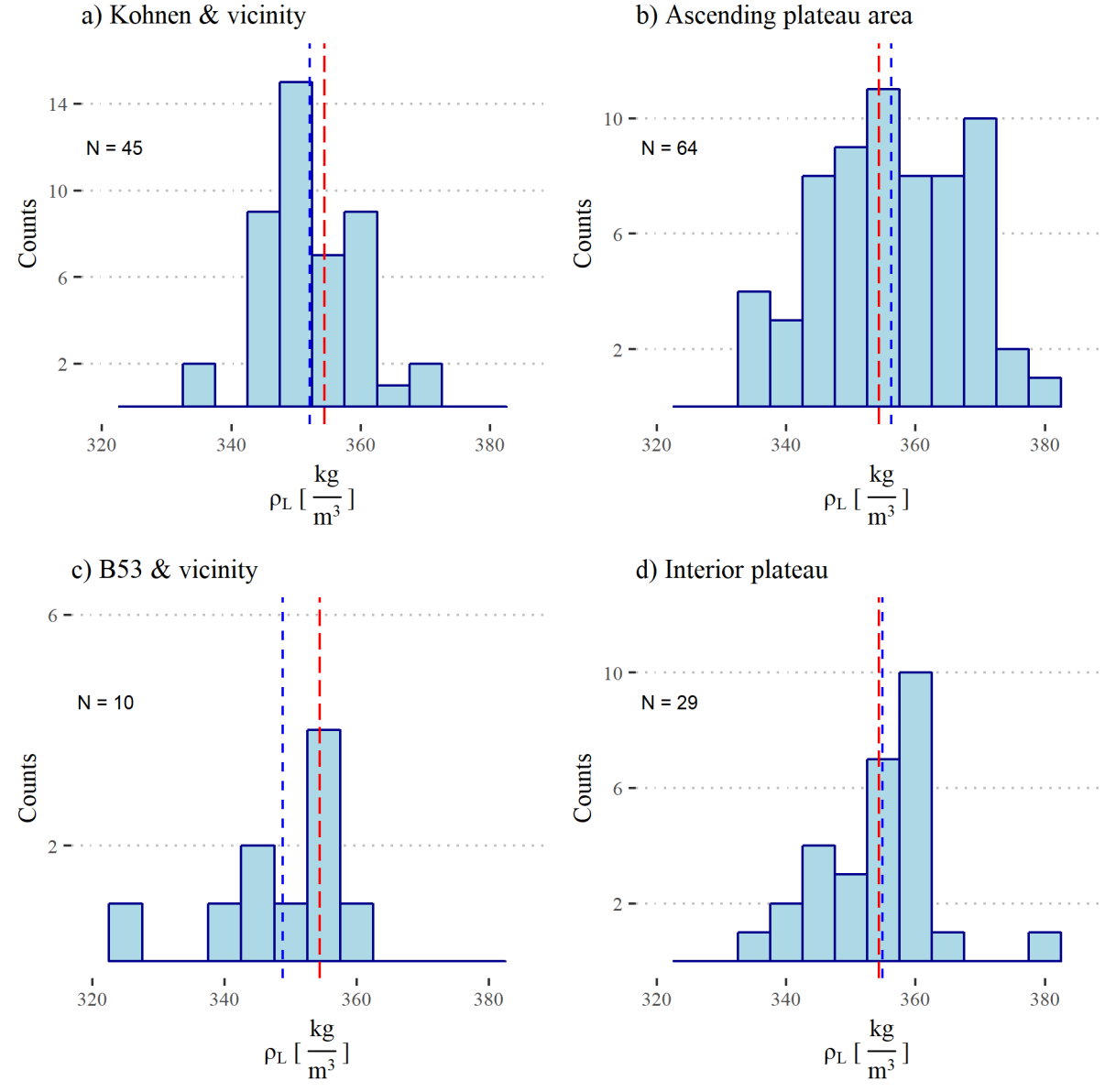

Figure 8: Histograms of the liner means for the four subareas (Fig. 1). The bin width for each histogram is 5 kg m^{-3}. The average ρ_L (Fig. 6, a) is given in a red dashed line while the liner mean of the respective subarea is marked with a blue dashed line.

Looking at the density distribution of the high resolution µCT density profiles (see Appendix) over one meter depth, we find a normal distribution of the snow density in the first meter (Fig. 9). We calculated the confidence interval (95%) of ρ_L for each respective subarea (Tab. 3). We want to stress that the number of samples of "B53 & vicinity" is lower than recommended for this method. The mean value for the traverse is represented in all four intervals of the subareas. We note, that the interval for

https://doi.org/10.5194/tc-2020-14
Preprint. Discussion started: 2 March 2020

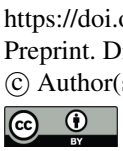

Kohnen & vicinity just includes this value. We used the same approach for the OIR trench and find, that the traverse mean is not represented here.

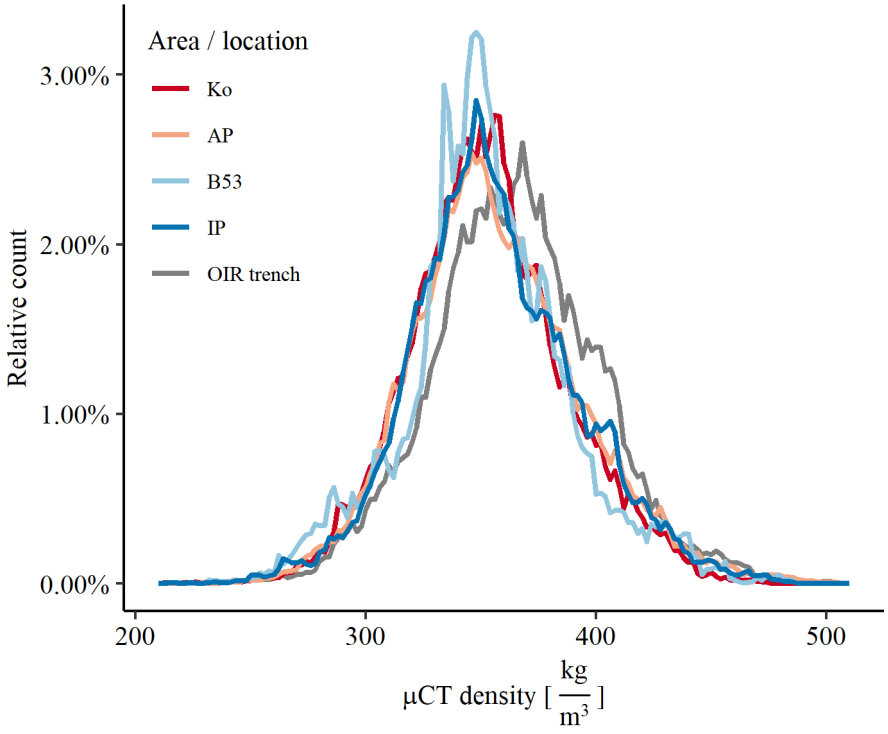

Figure 9: Density distribution from surface to one meter depth of the µCT density. It is based on all available liners - 114 liners from the traverse (according to their subarea), 30 liners for the OIR trench (grey) and 16 liners from Kohnen station (not this study) with a bin width of 2 kg m^{-3}. We used the same color code for the subareas (Sec. 2.5) as in Fig. 1. We find a shift towards higher densities in the OIR trench and a higher probability for lower densities in B53 & vicinity, but in general a similar distribution of density is found.

Table 3: Confidence intervals of 95% for each pooled area.

Area (number of samples)	*Lower boundary [kg m^{-3}]*	*Upper boundary [kg m^{-3}]*
Whole traverse (114)	352	356
Kohnen & vicinity (45)	350	354
Ascending plateau area (64)	353	358
B53 & vicinity (10)	341	357
Interior plateau (29)	351	358
OIR trench (30)	361	368

The snow density directly measured at the surface in general shows high spatial variability (Figs. 5 & 10). To characterize the spatial variability of density in a given area (tens of meters for traverse locations and trenches, hundreds of meters for Kohnen station), we use the parameter σ_H. For a comparison we used snow liners along the traverse (liners sampled at OIR trench

https://doi.org/10.5194/tc-2020-14
Preprint. Discussion started: 2 March 2020

presented in a separate column), liners from Kohnen station (Schaller, 2018) and from East Greenland ice core project (EGRIP) camp site (75°37′N, 35°59′W; 2702 m asl). We also calculated the σ_V for the respective areas, which can be interpreted as temporal (seasonal or annual) variations in density. We computed both (σ_H and σ_V) for 0.1 m, 0.5 m and 1 m intervals each (Tab. 4).

Table 4: Comparison of σ (horizontal and vertical) for each depth interval (from surface to respective depth) of samples from the traverse and OIR trench (this study), Kohnen and a trench from EGRIP (Schaller, 2018). Along the traverse we calculated the mean of the standard deviation at each location.

$\sigma^{0\text{-}X}$ [kg m^{-3}]	σ_V per loc. traverse	σ_H per loc. traverse	σ_V OIR trench	σ_H OIR trench	σ_V Kohnen	σ_H Kohnen	σ_V EGRIP trench	σ_H EGRIP trench
0.1 m	24	23	19	25	31	23	24	17
0.5 m	33	11	33	14	31	9	33	9
1.0 m	34	8	34	10	33	6	43	7

3.5 Small scale topography on OIR camp and Plateau Station

We find significant differences in the surface topography at both places. At OIR camp the height differences between the lowest and highest point of the measured transects are 60% larger than the height differences at Plateau Station (Tab. 5). The variation of height differences between the six transects at each location is low with a standard deviation of 2.4 cm (OIR camp) and 2.0 cm (Plateau Station).

Table 5: Maximum height differences [m] along the transects one to six at Plateau Station and B56

	1	2	3	4	5	6	Mean
OIR camp	0.268	0.280	0.310	0.330	0.319	0.310	0.303
Plateau Station	0.180	0.211	0.180	0.174	0.150	0.212	0.184

4 Discussion

4.1 Liner method vs. discrete sampling

To discuss the precision of 1 m liner mean density using the snow liner technique, we compare our dataset with data by Oerter (2008). In that study, snow pits with 20 km spacing have been dug and sampled along a small transect from Kohnen station upstream towards B51 (comp. Fig. 1). A detailed map of the sampled region is available in Huybrechts et al. (2007). Snow density has been measured volumetrically in each snow pit using discrete samples in 0.1 m depth intervals. We compare our results with density data from locations 1 to 4 (including single snow profiles in between) in two different depth resolutions (0.1 m & 1 m). For our study, we use $\rho^{0.1m}{}_{\mu CT}$ and ρ_L. For the 1 m interval from Oerter (2008) we use the average of all density values between 0 and 1 m.

https://doi.org/10.5194/tc-2020-14
Preprint. Discussion started: 2 March 2020

ρ^{1m} from both studies are in good agreement with each other. ρ^{1m} derived with the liner method tends to be 1-5% higher than the one from Oerter (2008) (Fig. 10). Higher discrepancy can be seen in the mean density of the upper 0.1 m. While we find on average $\rho^{0.1m}{}_{\mu CT}$=349 kg m^{-3} from liner measurements, $\rho^{0.1m}$ for Oerter (2008) is 293 kg m^{-3}. The calculated $\sigma^{0.1m}{}_{H}$ over the whole distance is 31 kg m^{-3} for our study and 25 kg m^{-3} for Oerter (2008). Interestingly, $\rho^{0.1m}$ in Oerter (2008) is always lower than ρ^{1m}, which is not the case in samples from our study. Due to the soft and unconsolidated snow at the surface we assume that the under-sampling error is higher at the surface for small sampling devices, which forces a systematic error towards smaller values (Fig. 10). Snow in greater depth has undergone sintering processes and is more coherent, therefore also the under-sampling error should be smaller. Additionally, a systematic error with increasing depth in the data by Oerter (2008) cannot be excluded, as the sampling device (core cutter) might densify the snow with each interval due to the thick wall in relation to the sampling volume. In contrast to other devices, the liner method preserves the original stratigraphy of the snow column, which results in a more precise density value in combination with the µCT-measurement on different chosen depth intervals, especially for small sampling intervals at the snow surface.

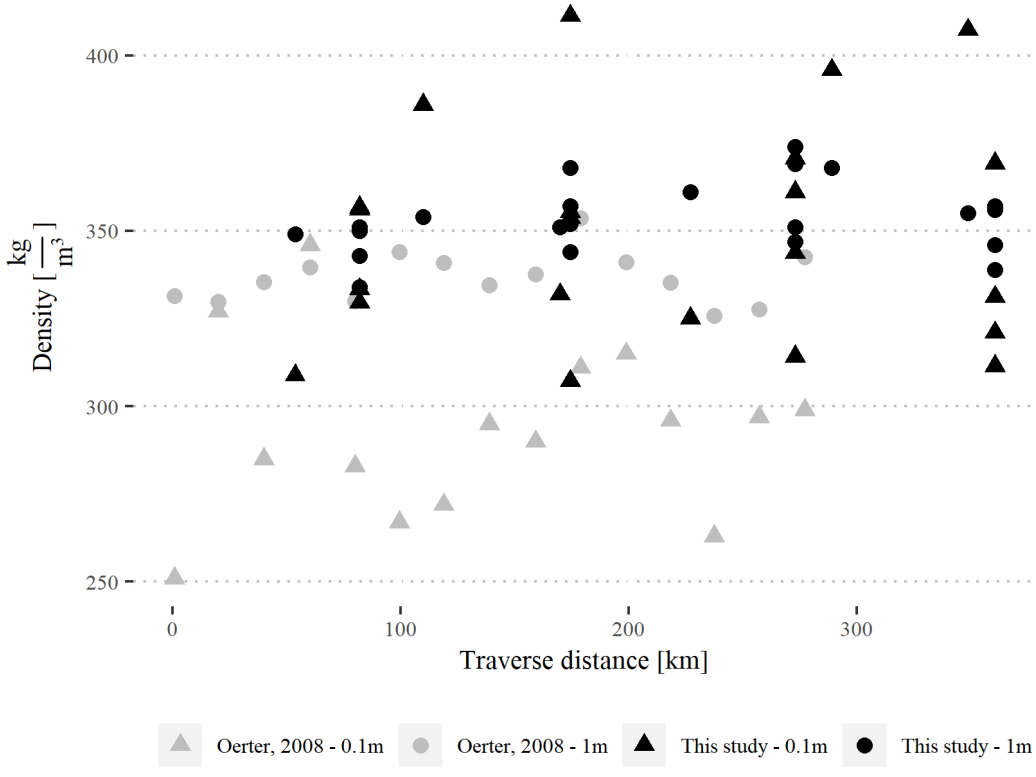

Figure 10: Density values of this study (black) in comparison with those from snow pit sampling by Oerter (2008) (grey). The samples are taken along a comparable transect line. Density is given as mean value from the snow surface to the respective depth. The spatial variability in both, 1 m and 0.1 m intervals, can be seen by the spread of points in data of this study at one sampling location (comp. Tab. 3).

https://doi.org/10.5194/tc-2020-14
Preprint. Discussion started: 2 March 2020

At sites with accumulation rates higher than 100 kg m^{-2} a^{-1}, small sampling intervals (<0.5 m) do not contain the seasonal or annual variability over several years (see data by Oerter (2008) in Fig. 10), at sites with low accumulation (<80 kg m^{-2} a^{-1}) the density might be masked by the high spatial heterogeneity. Both effects can be seen in the low $\sigma^{0.1\,m}{}_V$ in contrast to $\sigma^{1m}{}_V$ looking at data from different sites in Tab. 4. Higher $\sigma^{1m}{}_V$ in snow profiles from EGRIP are caused by a clearer seasonal density cycle, which is barely or not detectable on the EAP. This can be explained with warmer temperatures as well as higher accumulation rates at EGRIP. In case of surface melting (like in year 2012), $\sigma^{1m}{}_V$ can be even higher.

We find lower σ_H at the surface in samples from EGRIP in contrast to EAP. This can be explained with the non-uniform deposition causing a high surface topography. We measured the topography in form of dune heights (Tab. 5), which exceed the yearly accumulation by far. Snow layers do not form as spatially consistent as at sites, where the (predicted) yearly layer thickness is larger than the amplitude of dunes. This also affects the snow density as the signal cannot form homogenously over a larger distance and causes larger σ_H. The 0.1 m surface snow density has a 2.4 – 4 times higher σ_H than the 1 m interval. Furthermore, we want to advert to the time efficiency of the liner method. A 1 m snowpack density with four samples can be determined within 1 h. Even if a high resolution study in a snow pit is done, a snow profile using a liner can always be added to the discrete sampling in the snow pit as comparison. For these reasons, we suggest the 1 m liner mean density as the most feasible and precise method to derive a representative surface snow density on small scales.

4.2 Vertical and temporal variation of density along the traverse

Despite of errors due to the precision of the sampling method, the discrepancy in surface density between this study and Oerter (2008) can also be caused by the natural variability of snow density, which can be significant in consecutive years (Vihma et al., 2011). Also long-term changes in temperature, accumulation rate or wind systems can affect fluctuations in density. Several recent studies postulate an increase in temperature and accumulation rate in some areas in Antarctica, partly also on the EAP (Medley and Thomas, 2019). But precise accumulation rates for the interior EAP are hard to determine and are generally overestimated (Anschütz et al., 2011).

We test the impact on surface snow density of a 1°C temperature rise, which has been recorded at Kohnen station with an automatic weather station (AWS) over the past 20 years and discussed by Medley et al. (2018), and a 15% overestimation of the accumulation rate on the interior plateau. The temperature dependent densification effect can be neglected in that context. According to the model by Herron and Langway (1980), at a temperature of -44.6°C (annual mean air temperature at Kohnen station (Oerter et al., 1999)), the increase in snow density by densification from the surface to 1 m depth is 10 kg m^{-3}. At a -54.6°C annual mean air temperature (-10°C compared to Kohnen station) the densification is roughly 8.3 kg m^{-3}. A temperature change of -1°C would lower the densification induced density by about 0.17 kg m^{-3}.

We use the parameterization after Sugiyama et al. (2012):

$$\rho = 305 + 0.629\,T + 0.150\,\dot{A} + 13.5\,W, \quad (1)$$

where T is the annual mean temperature [°C], $\dot{A}$ the accumulation rate [mm we a^{-1}] (we water equivalent) and W the mean wind speed [ms^{-1}] at the given location. We use an annual mean temperature of -50°C, an accumulation rate of 40 mm we a^{-1} and a

https://doi.org/10.5194/tc-2020-14
Preprint. Discussion started: 2 March 2020

wind speed of 4 m s^{-1}, roughly the mean values of the area covered with the traverse. We get an increase in density of 0.6 kg m^{-3} °C $^{-1}$ and ±1.2 kg m^{-3} for ±8 mm we a^{-1}. As both potential increases (decreases, respectively) are inside the error range and are masked by the sampling error, we cannot attribute a change in density to a potential temperature (or accumulation rate) change. In general we conclude, that several parameterizations for the surface snow density (Kaspers et al., 2004; Sugiyama et al., 2012) need further tuning for regions with low accumulation and low temperatures like the EAP.

The uniform density distribution of density over 1 m for the respective subsets (Fig. 9) also indicates, that the natural variability of the snow density is larger than the change of environmental conditions we find along the traverse on EAP. Only ρ in the OIR trench is higher than the average of the four areal subsets. A possible explanation is the direction dependent sampling in the OIR trench, as the wind direction can have an influence on the correlation of snow profiles (Schaller, 2018). In contrast to the OIR trench, profiles at the locations along the traverse were taken in three directions from a common center, independently from the predominant wind direction (Fig 2).

4.3 Error assessment of SMB

Sasgen et al. (2019) calculated from a combination of the Gravity Recovery and Climate Experiment (GRACE) and CryoSat-2 a mass balance for Antarctica of -178±23 Gt a^{-1}. We try a simple quantitative calculation of the underestimated water equivalent in the firn column with the density data presented in this study (average ρ_{loc}) using the semi-empirical firn densification model by Herron and Langway (1980). We use an annual mean temperature of -50°C and an accumulation rate of 0.04 m we a^{-1}, roughly the mean values of the area covered with the traverse. We use the two surface densities $\rho_0(1)$=320 kg m^{-3} and $\rho_0(2)$=355 kg m^{-3}.

We calculated 59.0 m we for $\rho_0(1)$ and 61.0 m we for $\rho_0(2)$ in the firn colum, reaching the critical density of the firn-ice-transition at 830 kg m^{-3} in 92.9 m. The calculation is in good agreement with firn density (µCT) measured in core B53 (unpublished). This is roughly an underestimation in mass of 3%. Other effects like an overestimation of the accumulation rate on the interior plateau are not taken into account. Extrapolating this underestimation to the East Antarctic ice sheet using the sea level equivalent for East Antarctica after Rignot et al. (2019) and an average ice sheet thickness of 2 km, this 3% mass underestimation corresponds to 5 cm sea level equivalent.

4.4 A representative surface snow density on the EAP

In order to overcome the sparsity of in-situ observations of surface snow density, regional climate models and derivatives with adequate snow deposition modules are often used to obtain estimates of surface accumulation and density on a full regional scale. Compared to the firn model presented by Ligtenberg et al. (2011), we find systematically higher values for density on the interior EAP than the model predicts for the same locations. While ρ_{loc} spans the range from 346 to 372 kg m^{-3}, the firn model provides a range from 308 to 332 kg m^{-3} (Fig. 11). Having a sound statistics at these locations, we exclude the systematic bias to be caused by our observations, but rather a shortcoming of the model to yield densities which are about 10% too low. This could be caused by a multitude of reasons, e.g. model physics, spatial and temporal resolution or forcing. We suggest to

https://doi.org/10.5194/tc-2020-14
Preprint. Discussion started: 2 March 2020

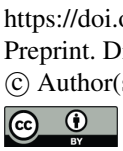

set up a specific model test designed for the EAP and use data sets like ours and those from comparable studies as the standard against which to evaluate model outcomes.

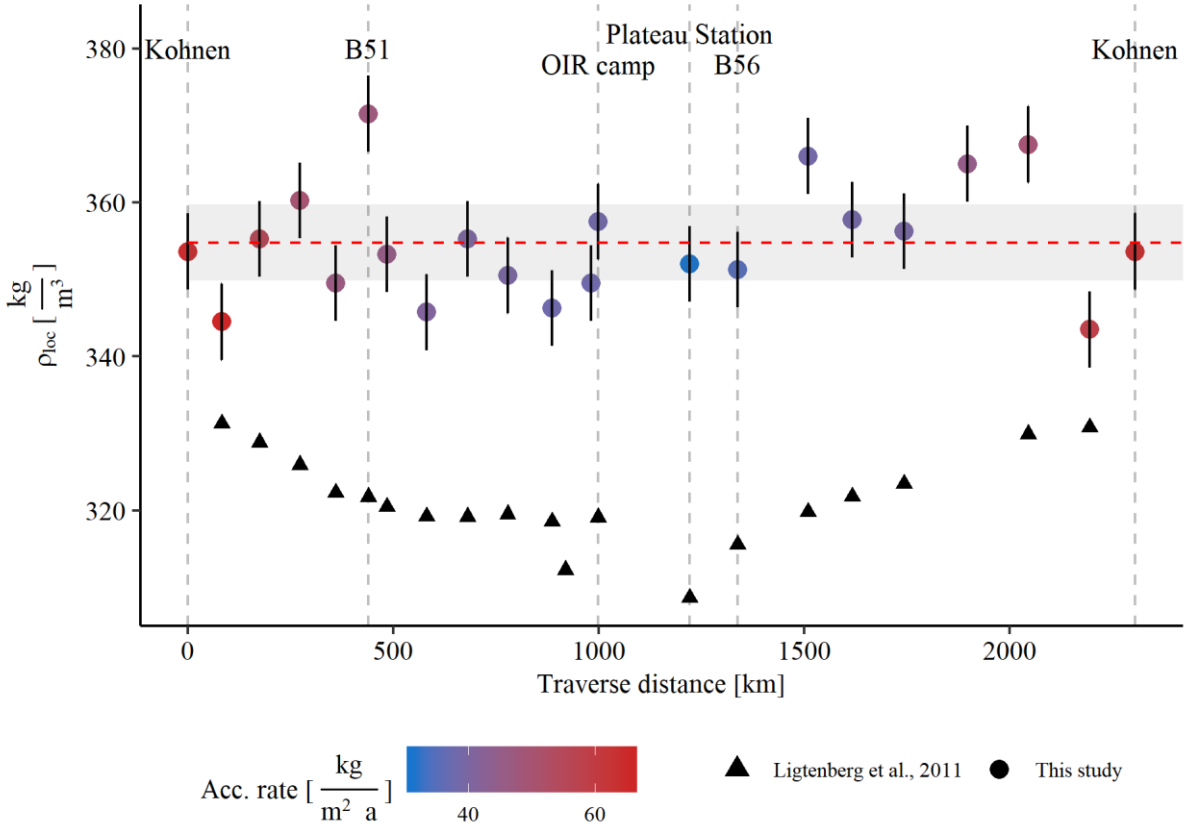

Figure 11: ρ_{loc} along one leg of the traverse route, from Kohnen to B51, further along the ice divide to B53 and from Plateau Station straight back to Kohnen station. σ_n calculated from the OIR trench (Sect. 3.3) is given by vertical error bars at each location. A mean density value for Kohnen station was calculated from samples not collected in this study (s. 2.5). The red dashed horizontal line indicates the mean density along the whole traverse, σ_n is indicated with a grey shade. The color code shows the accumulation rate according to Arthern et al. (2006). Only locations with multiple liners are shown here. The triangles show the parameterized density values according to Ligtenberg et al. (2011).

We cannot detect a clear trend in density along the whole traverse route. A potential reason might be the increase in elevation and decrease in temperature as well as accumulation rate (Fig. 11), as the distance to the coast and major Dronning Maud Land (DML) ice divide increases as well. But our observation is consistent with recent field observations on the EAP (Sugiyama et al., 2012) or snow density collections from over two decades (Tian et al., 2018). Sugiyama et al. (2012) found a density around 350 kg m^{-3} for the same depth interval (0-1 m) along a traverse between Dome F and Kohnen station, with a similar spatial variability.

Still we can spot patterns on large scales. We explain the increase in surface density along the ice divide from Kohnen towards B51 (Figs. 8, b & 11) by the increasing influence of katabatic winds, blowing from the Plateau along surface slope gradient to

https://doi.org/10.5194/tc-2020-14
Preprint. Discussion started: 2 March 2020

the coastal regions. The observation of this systematic change in density is also visible in Sugiyama et al. (2012) and not captured by firn models. In fact, the model by Ligtenberg et al. (2011) shows the opposite trend along this traverse section (km 0-500 in Fig. 11). High density at B51 goes along with stronger dune formation than at Kohnen station, which was observed to increase along this traverse part. This is consistent with observations of dune formation at wind speed exceeding 10 m s^{-1} (Birnbaum et al., 2010). Modelled density is mainly parameterized by wind speed, but the process of snow redistribution might be underestimated. We assume that the relatively low density values – at least in comparison within our dataset – for the locations 14 and 15 (Plateau Station and B56, Fig. 11) in the calm accumulation zone, are most likely caused by snow redistribution. The relatively low wind speed (Lenaerts and van den Broeke, 2012), in combination with low temperatures and humidity (Picciotto et al., 1971), is not high enough to cause wind packing and sintering of snowflakes. It rather redistributes them smoothly at the surface, which also happens at low wind speeds. Therefore, as the sintering process is prolongated, we find lower snow density at these locations. But as the low densities cannot be seen for the whole interior plateau region (Fig. 8, d), we consider it rather as a process that needs very specific settings on the high plateau than an average characteristic. The abundance of wind speeds higher than 10 m s^{-1} might be a limiting factor in this context. We want to stress, that also the modelled density reaches its minimum at Plateau Station. Different environmental conditions at B53 & vicinity might cause lower density here as well (Fig. 8, c). High σ_n for subset B53 & vicinity should not be over-interpreted, as only one sampling location with four profiles is present there. Still σ_{loc} is highest here amongst all locations with multiple liners along the traverse (comp. also σ^{1m}_H in Tab. 2). An explanation can be a different wind and accumulation regime at the distant side of the ice divide causing high heterogeneity on a very small scale.

Small fluctuations in density within the error range at nearby locations can be explained by local noise (Laepple et al., 2016; Münch et al., 2016). Stronger variations in density, e.g. beyond a standard variation, can be caused by a complex interaction between wind speed and surface roughness on the small scale but have also shown to originate from dynamic interaction of ice flow over bedrock undulations, thus altering surface slope and in turn elevation and accumulation rate on the large scale in this region (Eisen et al., 2005; Rotschky et al., 2004).

As already stated above we cannot conclusively attribute a cause to the model behavior. Unfortunately, it is also difficult to pin down the mechanism for the observed systematic spatial distribution of density. Obviously, a dedicated sensitivity study with a snow deposition and firn model is needed to discriminate the various effects affecting postdepositional snow metamorphism and densification.

5 Conclusion

We presented surface snow density data along a traverse route from Kohnen station to former Plateau Station on the EAP using the time efficient liner method. Compared to other discrete sampling techniques, which have a sampling error up to ±4% (Conger and McClung, 2009), the liner technique (this study and e.g. Schaller et al., 2016) possesses a precision of less than 2% relative error for a 1 m mean snow density. It covers seasonal and annual variations at sites of high accumulation and

https://doi.org/10.5194/tc-2020-14
Preprint. Discussion started: 2 March 2020

reduces the influence of high surface roughness in relation to the annual accumulation in low accumulation areas. We compared snow profiles to density data from snow pits by Oerter (2008). We found a 1-5% discrepancy for the 1 m density, which cannot be attributed to a temperature change between the sampling dates. For the density from surface to 0.1 m depth we find a considerable 16% difference in density, that we explain with a systematic sampling error. This systematic error makes comparisons of old and new datasets with different sampling devices difficult, as an increase in mass in Antarctica or an underestimation of mass in the past is difficult to detect. As Alexander et al. (2019) pointed out, errors or biases in 1 m snow density can lead to large uncertainties in SMB. Especially on the EAP, in-situ data are sparse. A representative surface snow density is needed for a precise determination of the surface snow density in a given area. We conclude, that four spatially independent snow profiles are necessary to determine a snow density value with an error lower than 1.5% of the mean. To further verify this result in future studies, we suggest to test this with a similar sampling scheme with five and more profiles using the liner technique. A circular setup with one profile in the midpoint and four to six profiles along a circle with a radius of 10 m to keep spatial independency might be a feasible approach.

With the volumetrically calculated 1 m mean snow density we confirm earlier density observations (Sugiyama et al., 2012) and suggest a representative mean density of 355 kg m^{-3} for surface snow on regional scales on the EAP. On smaller, subregional scales closer to the coast and thus more subject to the synoptic influence of low-pressure systems, systematic linear trends are visible, which we attribute to the effect of katabatic winds. As we find a high variability on different spatial scales, we suggest to average point measurements for snow density over regional scales to find a spatially representative density value for the surface instead of using single measurements. We divided the area covered by the traverse into subareas due to different environmental regimes, but we cannot find significant differences in snow density among them. Natural variability in snow density seems to be higher than previously assumed. Especially on the regional scale, we cannot see a clear correlation between temperature and accumulation rate with snow density. For future studies we therefore suggest to sample transects of 50-100 km with samples every 1 km to investigate the influence of topography changes on snow density in more detail.

We also suggest further tuning for parameterizations of the surface snow density, especially for regions with environmental conditions like the EAP. We calculated that an underestimation of the surface snow density (in our case 320 kg m^{-3} instead of 355 kg m^{-3}) using the model by Herron and Langway (1980) can lead to a 3% mass underestimation in the firn column, which roughly corresponds to 5 cm sea level equivalent. Compared to recent calculations from GRACE and CryoSat-2 where the SMB is given with a 13% error estimation (Sasgen et al., 2019), our data can be used to update density parameterizations and therefore sustainably improve SMB estimates.

6 Data availability

Datasets will be uploaded to the open-access repository Pangaea.

https://doi.org/10.5194/tc-2020-14
Preprint. Discussion started: 2 March 2020

7 Author contributions & conflict of interest

JF and SK were in charge for the planning of the scientific expedition. AW and SK took the snow liners along the traverse. AW conducted the majority of the μCT measurements, performed the analysis and wrote the manuscript. JF discussed the preliminary results with the main author, suggested further strategies and reviewed the manuscript. MH, SK and OE improved the manuscript with helpful feedback.

OE is Co-Editor-in-Chief of The Cryosphere.

8 Acknowledgements

We want to thank the whole logistic team of the traverse for technical support during the expedition and Alexandra Touzeau for assisting at taking snow liners in the field. Thanks to Melissa Mengert for conducting parts of the μCT measurements, Christoph Schaller and Ludwig Schroeder for interesting discussions and Thomas Laepple for sharing his experience regarding representativity of climate proxies.

Alexander Weinhart is funded by the German environmental foundation (Deutsche Bundesstiftung Umwelt).

9 References

Agosta, C., Amory, C., Kittel, C., Orsi, A., Favier, V., Gallée, H., van den Broeke, M. R., Lenaerts, J. T. M., van Wessem, J. M., van de Berg, W. J., and Fettweis, X.: Estimation of the Antarctic surface mass balance using the regional climate model MAR (1979–2015) and identification of dominant processes, The Cryosphere, 13, 281-296, 2019.

Alexander, P. M., Tedesco, M., Koenig, L., and Fettweis, X.: Evaluating a Regional Climate Model Simulation of Greenland Ice Sheet Snow and Firn Density for Improved Surface Mass Balance Estimates, Geophysical Research Letters, 46, 12073-12082, 2019.

Anschütz, H., Sinisalo, A., Isaksson, E., McConnell, J. R., Hamran, S. E., Bisiaux, M. M., Pasteris, D., Neumann, T. A., and Winther, J. G.: Variation of accumulation rates over the last eight centuries on the East Antarctic Plateau derived from volcanic signals in ice cores, Journal of Geophysical Research-Atmospheres, 116, 12, 2011.

Arthern, R. J., Winebrenner, D. P., and Vaughan, D. G.: Antarctic snow accumulation mapped using polarization of 4.3-cm wavelength microwave emission, Journal of Geophysical Research-Atmospheres, 111, 10, 2006.

Birnbaum, G., Freitag, J., Brauner, R., Konig-Langlo, G., Schulz, E., Kipfstuhl, S., Oerter, H., Reijmer, C. H., Schlosser, E., Faria, S. H., Ries, H., Loose, B., Herber, A., Duda, M. G., Powers, J. G., Manning, K. W., and van den Broeke, M. R.: Strong-wind events and their influence on the formation of snow dunes: observations from Kohnen station, Dronning Maud Land, Antarctica, Journal of Glaciology, 56, 891-902, 2010.

Conger, S. M. and McClung, D. M.: Comparison of density cutters for snow profile observations, Journal of Glaciology, 55, 163-169, 2009.

Eisen, O., Rack, W., Nixdorf, U., and Wilhelms, F.: Characteristics of accumulation around the EPICA deep-drilling site in Dronning Maud Land, Antarctica, Annals of Glaciology, Vol 41 2005, 41, 41-46, 2005.

Fisher, D. A., Reeh, N., and Clausen, H. B.: Stratigraphic noise in time series derived from ice cores, Annals of Glaciology, 7, 76-83, 1985.

Freitag, J., Kipfstuhl, S., and Laepple, T.: Core-scale radioscopic imaging: a new method reveals density–calcium link in Antarctic firn, Journal of Glaciology, 59, 1009-1014, 2013.

Frezzotti, M., Gandolfi, S., La Marca, F., and Urbini, S.: Snow dunes and glazed surfaces in Antarctica: new field and remote-sensing data, Annals of Glaciology, Vol 34, 2002, 34, 81-88, 2002.

Fujita, S., Holmlund, P., Andersson, I., Brown, I., Enomoto, H., Fujii, Y., Fujita, K., Fukui, K., Furukawa, T., Hansson, M., Hara, K., Hoshina, Y., Igarashi, M., Iizuka, Y., Imura, S., Ingvander, S., Karlin, T., Motoyama, H., Nakazawa, F., Oerter, H., Sjoberg, L. E., Sugiyama, S., Surdyk, S., Strom, J., Uemura, R., and Wilhelms, F.: Spatial and temporal variability of snow accumulation rate on the East Antarctic ice divide between Dome Fuji and EPICA DML, Cryosphere, 5, 1057-1081, 2011.

Furukawa, T., Kamiyama, K., and Maeno, H.: Snow surface features along the traverse route from the coast to Dome Fuji Station, Queen Maud Land, Antarctica, Proceedings of the NIPR Symposium on Polar Meteorology and Glaciology, 10, 13-24, 1996.

https://doi.org/10.5194/tc-2020-14
Preprint. Discussion started: 2 March 2020

Herron, M. M. and Langway, C. C.: Firn Densification - an Empirical-Model, Journal of Glaciology, 25, 373-385, 1980.
Huybrechts, P., Rybak, O., Pattyn, F., Ruth, U., and Steinhage, D.: Ice thinning, upstream advection, and non-climatic biases for the upper 89% of the EDML ice core from a nested model of the Antarctic ice sheet, Climate of the Past, 3, 577-589, 2007.
IPCC: IPCC Special Report on the Ocean and Cryosphere in a Changing Climate. Pörtner, H.-O., Roberts, D. C., Masson-Delmotte, V., Zhai, P., Tignor, M., Poloczanska, E., Mintenbeck, K., Alegría, A., Nicolai, M., Okem, A., Petzold, J., Rama, B., and Weyer, N. M. (Eds.), 2019.
Karlsson, N. B., Binder, T., Eagles, G., Helm, V., Pattyn, F., Van Liefferinge, B., and Eisen, O.: Glaciological characteristics in the Dome Fuji region and new assessment for "Oldest Ice", Cryosphere, 12, 2413-2424, 2018.
Kaspers, K. A., van de Wal, R. S. W., van den Broeke, M. R., Schwander, J., van Lipzig, N. P. M., and Brenninkmeijer, C. A. M.: Model calculations of the age of firn air across the Antarctic continent, Atmos. Chem. Phys., 4, 1365-1380, 2004.
Konrad, H., Sasgen, I., Pollard, D., and Klemann, V.: Potential of the solid-Earth response for limiting long-term West Antarctic Ice Sheet retreat in a warming climate, Earth and Planetary Science Letters, 432, 254-264, 2015.
Laepple, T., Hörhold, M., Münch, T., Freitag, J., Wegner, A., and Kipfstuhl, S.: Layering of surface snow and firn at Kohnen Station, Antarctica: Noise or seasonal signal?, Journal of Geophysical Research-Earth Surface, 121, 1849-1860, 2016.
Lenaerts, J. T. M., Medley, B., van den Broeke, M. R., and Wouters, B.: Observing and Modeling Ice Sheet Surface Mass Balance, Reviews of Geophysics, 57, 376-420, 2019.
Lenaerts, J. T. M. and van den Broeke, M. R.: Modeling drifting snow in Antarctica with a regional climate model: 2. Results, Journal of Geophysical Research: Atmospheres, 117, n/a-n/a, 2012.
Ligtenberg, S. R. M., Helsen, M. M., and van den Broeke, M. R.: An improved semi-empirical model for the densification of Antarctic firn, Cryosphere, 5, 809-819, 2011.
McMillan, M., Shepherd, A., Sundal, A., Briggs, K., Muir, A., Ridout, A., Hogg, A., and Wingham, D.: Increased ice losses from Antarctica detected by CryoSat-2, Geophysical Research Letters, 41, 3899-3905, 2014.
Medley, B., McConnell, J. R., Neumann, T. A., Reijmer, C. H., Chellman, N., Sigl, M., and Kipfstuhl, S.: Temperature and Snowfall in Western Queen Maud Land Increasing Faster Than Climate Model Projections, Geophysical Research Letters, 45, 1472-1480, 2018.
Medley, B. and Thomas, E. R.: Increased snowfall over the Antarctic Ice Sheet mitigated twentieth-century sea-level rise, Nature Climate Change, 9, 34-+, 2019.
Münch, T., Kipfstuhl, S., Freitag, J., Meyer, H., and Laepple, T.: Regional climate signal vs. local noise: a two-dimensional view of water isotopes in Antarctic firn at Kohnen Station, Dronning Maud Land, Climate of the Past, 12, 1565-1581, 2016.
Oerter, H.: High resolution density and d18O of snow pits DML76S05_11 to DML90S05_25. Oerter, H., Fischer, H., and Sperlich, P. (Eds.), Pangaea, 2008.
Oerter, H., Graf, W., Wilhelms, F., Minikin, A., and Miller, H.: Accumulation studies on Amundsenisen, Dronning Maud Land, Antarctica, by means of tritium, dielectric profiling and stable-isotope measurements: first results from the 1995-96 and 1996-97 field seasons, Ann Glaciol, 29, 1-9, 1999.
Picciotto, E., Crozaz, G., and De Breuck, W.: Accumulation on the South Pole-Queen Maud Land Traverse, 1964-1968, doi: 10.1029/AR016p0257, 1971. 257-315, 1971.
Proksch, M., Lowe, H., and Schneebeli, M.: Density, specific surface area, and correlation length of snow measured by high-resolution penetrometry, Journal of Geophysical Research-Earth Surface, 120, 346-362, 2015.
Rignot, E., Mouginot, J., Scheuchl, B., van den Broeke, M., van Wessem, M. J., and Morlighem, M.: Four decades of Antarctic Ice Sheet mass balance from 1979-2017, Proc. Natl. Acad. Sci. U. S. A., 116, 1095-1103, 2019.
Rotschky, G., Eisen, O., Wilhelms, F., Nixdorf, U., and Oerter, H.: Spatial distribution of surface mass balance on Amundsenisen plateau, Antarctica, derived from ice-penetrating radar studies, Ann Glaciol-Ser, 39, 265-270, 2004.
Sasgen, I., Konrad, H., Helm, V., and Grosfeld, K.: High-Resolution Mass Trends of the Antarctic Ice Sheet through a Spectral Combination of Satellite Gravimetry and Radar Altimetry Observations, Remote Sens., 11, 144, 2019.
Sasgen, I., Konrad, H., Ivins, E. R., Van den Broeke, M. R., Bamber, J. L., Martinec, Z., and Klemann, V.: Antarctic ice-mass balance 2003 to 2012: regional reanalysis of GRACE satellite gravimetry measurements with improved estimate of glacial-isostatic adjustment based on GPS uplift rates, Cryosphere, 7, 1499-1512, 2013.
Schaller, C. F.: Towards understanding the signal formation in polar snow, firn and ice using X-ray computed tomography, PhD Thesis, Department of Geosciences, University Bremen, Bremen, 2018.
Schaller, C. F., Freitag, J., Kipfstuhl, S., Laepple, T., Steen-Larsen, H. C., and Eisen, O.: A representative density profile of the North Greenland snowpack, Cryosphere, 10, 1991-2002, 2016.
Schroder, L., Horwath, M., Dietrich, R., Helm, V., van den Broeke, M. R., and Ligtenberg, S. R. M.: Four decades of Antarctic surface elevation changes from multi-mission satellite altimetry, Cryosphere, 13, 427-449, 2019.
Shepherd, A., Ivins, E., Rignot, E., Smith, B., van den Broeke, M., Velicogna, I., Whitehouse, P., Briggs, K., Joughin, I., Krinner, G., Nowicki, S., Payne, T., Scambos, T., Schlegel, N., Geruo, A., Agosta, C., Ahlstrom, A., Babonis, G., Barletta, V., Blazquez, A., Bonin, J., Csatho, B., Cullather, R., Felikson, D., Fettweis, X., Forsberg, R., Gallee, H., Gardner, A., Gilbert, L., Groh, A., Gunter, B., Hanna, E., Harig, C., Helm, V., Horvath, A., Horwath, M., Khan, S., Kjeldsen, K. K., Konrad, H., Langen, P., Lecavalier, B., Loomis, B., Luthcke, S.,

https://doi.org/10.5194/tc-2020-14
Preprint. Discussion started: 2 March 2020

McMillan, M., Melini, D., Mernild, S., Mohajerani, Y., Moore, P., Mouginot, J., Moyano, G., Muir, A., Nagler, T., Nield, G., Nilsson, J., Noel, B., Otosaka, I., Pattle, M. E., Peltier, W. R., Pie, N., Rietbroek, R., Rott, H., Sandberg-Sorensen, L., Sasgen, I., Save, H., Scheuchl, B., Schrama, E., Schroder, L., Seo, K. W., Simonsen, S., Slater, T., Spada, G., Sutterley, T., Talpe, M., Tarasov, L., van de Berg, W. J., van der Wal, W., van Wessem, M., Vishwakarma, B. D., Wiese, D., Wouters, B., and Team, I.: Mass balance of the Antarctic Ice Sheet from 1992 to 2017, Nature, 558, 219-+, 2018.

Shepherd, A., Ivins, E. R., A, G., Barletta, V. R., Bentley, M. J., Bettadpur, S., Briggs, K. H., Bromwich, D. H., Forsberg, R., Galin, N., Horwath, M., Jacobs, S., Joughin, I., King, M. A., Lenaerts, J. T., Li, J., Ligtenberg, S. R., Luckman, A., Luthcke, S. B., McMillan, M., Meister, R., Milne, G., Mouginot, J., Muir, A., Nicolas, J. P., Paden, J., Payne, A. J., Pritchard, H., Rignot, E., Rott, H., Sorensen, L. S., Scambos, T. A., Scheuchl, B., Schrama, E. J., Smith, B., Sundal, A. V., van Angelen, J. H., van de Berg, W. J., van den Broeke, M. R., Vaughan, D. G., Velicogna, I., Wahr, J., Whitehouse, P. L., Wingham, D. J., Yi, D., Young, D., and Zwally, H. J.: A reconciled estimate of ice-sheet mass balance, Science, 338, 1183-1189, 2012.

Sihvola, A. and Tiuri, M.: Snow fork for field determination of the density and wetness profiles of a snow pack, IEEE Trans. Geosci. Remote Sensing, 24, 717-721, 1986.

Sorensen, L. S., Simonsen, S. B., Langley, K., Gray, L., Helm, V., Nilsson, J., Stenseng, L., Skourup, H., Forsberg, R., and Davidson, M. W. J.: Validation of CryoSat-2 SARIn Data over Austfonna Ice Cap Using Airborne Laser Scanner Measurements, Remote Sens., 10, 12, 2018.

Stenni, B., Curran, M. A. J., Abram, N. J., Orsi, A., Goursaud, S., Masson-Delmotte, V., Neukom, R., Goosse, H., Divine, D., van Ommen, T., Steig, E. J., Dixon, D. A., Thomas, E. R., Bertler, N. A. N., Isaksson, E., Ekaykin, A., Frezzotti, M., and Werner, M.: Antarctic climate variability at regional and continental scales over the last 2,000 years, Climate of the Past Discussions, doi: 10.5194/cp-2017-40, 2017. 1-35, 2017.

Sugiyama, S., Enomoto, H., Fujita, S., Fukui, K., Nakazawa, F., Holmlund, P., and Surdyk, S.: Snow density along the route traversed by the Japanese-Swedish Antarctic Expedition 2007/08, Journal of Glaciology, 58, 529-539, 2012.

Tian, Y., Zhang, S., Du, W., Chen, J., Xie, H., Tong, X., and Li, R.: Surface Snow Density of East Antarctica Derived from in-Situ Observations, ISPRS - International Archives of the Photogrammetry, Remote Sensing and Spatial Information Sciences, XLII-3, 1657-1660, 2018.

van den Broeke, M.: Depth and density of the Antarctic firn layer, Arct. Antarct. Alp. Res., 40, 432-438, 2008.

Van Liefferinge, B., Pattyn, F., Cavitte, M. G. P., Karlsson, N. B., Young, D. A., Sutter, J., and Eisen, O.: Promising Oldest Ice sites in East Antarctica based on thermodynamical modelling, Cryosphere, 12, 2773-2787, 2018.

Vihma, T., Mattila, O. P., Pirazzini, R., and Johansson, M. M.: Spatial and temporal variability in summer snow pack in Dronning Maud Land, Antarctica, Cryosphere, 5, 187-201, 2011.

https://doi.org/10.5194/tc-2020-14
Preprint. Discussion started: 2 March 2020

10 Appendix

For a better understanding of Fig. 9, we show a density profile over depth measured with the µCT. In the radioscopic image the stratification of the snowpack is visible. In Fig. 9 we took all high resolution µCT density profiles along the traverse, according to their subarea, as well as the OIR trench and plotted the relative abundance of the density values in 2 kg m^{-3} intervals.

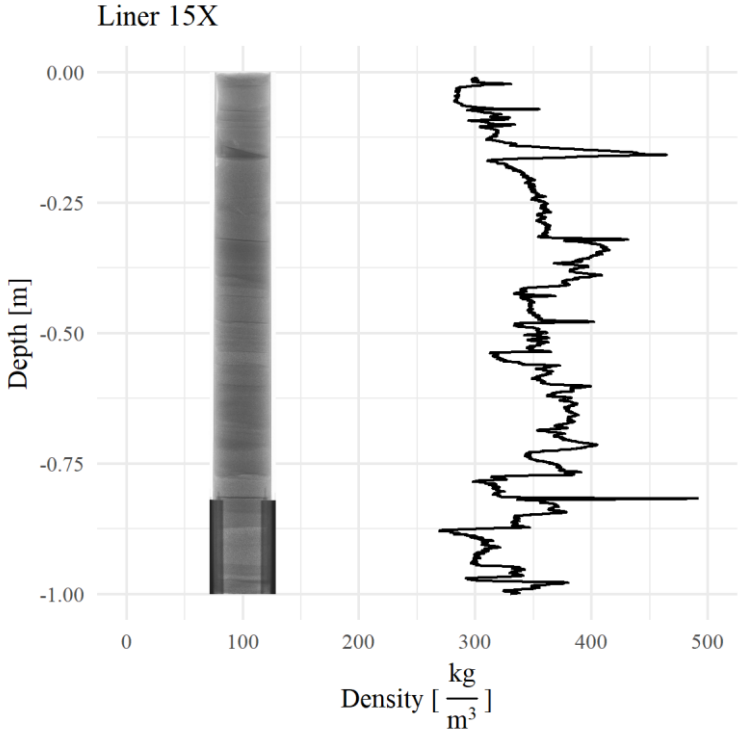

Figure 12: µCT density of a snow profile at position 15X. On the left the radioscopic image of the snow profile is visible. Dark grey colour represents high density, bright grey represents low density values. On the right, the corresponding density profile over depth is shown.